



Nonlinear electrophoretic velocity of a spherical colloidal particle

Richard Cobos¹ and Aditya S. Khair^{1,†}

¹Department of Chemical Engineering, Carnegie Mellon University, Pittsburgh, PA 15213, USA

(Received 29 January 2023; revised 14 May 2023; accepted 25 June 2023)

Electrophoresis is the motion of a charged colloidal particle in an electrolyte under an applied electric field. The electrophoretic velocity of a spherical particle depends on the dimensionless electric field strength $\beta = a^* e^* E_\infty^* / k_B^* T^*$, defined as the ratio of the product of the applied electric field magnitude E_∞^* and particle radius a^* , to the thermal voltage $k_B^* T^* / e^*$, where k_B^* is Boltzmann's constant, T^* is the absolute temperature, and e^* is the charge on a proton. In this paper, we develop a spectral element algorithm to compute the electrophoretic velocity of a spherical, rigid, dielectric particle, of fixed dimensionless surface charge density σ over a wide range of β . Here, $\sigma = (e^* a^* / \epsilon^* k_B^* T^*) \sigma^*$, where σ^* is the dimensional surface charge density, and ϵ^* is the permittivity of the electrolyte. For moderately charged particles ($\sigma = O(1)$), the electrophoretic velocity is linear in β when $\beta \ll 1$, and its dependence on the ratio of the Debye length ($1/\kappa^*$) to particle radius (denoted by $\delta = 1/(\kappa^* a^*)$) agrees with Henry's formula. As β increases, the nonlinear contribution to the electrophoretic velocity becomes prominent, and the onset of this behaviour is δ -dependent. For $\beta \gg 1$, the electrophoretic velocity again becomes linear in field strength, approaching the Hückel limit of electrophoresis in a dielectric medium, for all δ . For highly charged particles ($\sigma \gg 1$) in the thin-Debye-layer limit ($\delta \ll 1$), our computations are in good agreement with recent experimental and asymptotic results.

Key words: colloids, electrokinetic flows

1. Introduction

Electrophoresis is an electrokinetic phenomenon, in which a charged colloidal particle suspended in an electrolyte is set in motion by an applied electric field. Electrophoresis has applications in colloid science (Russel, Saville & Schowalter 1991), microfluidics (Erickson & Li 2004; Liu & Mathies 2009), DNA sequencing (Huang, Quesada & Mathies 1992), protein separation (Zhu, Lu & Liu 2012), active matter (De Corato *et al.* 2020) and directed assembly (Mittal *et al.* 2008), among others. The strength of the imposed

† Email address for correspondence: akhair@andrew.cmu.edu

electric field is characterized by the dimensionless parameter $\beta = a^* e^* E_\infty^* / k_B^* T^*$, for a spherical particle of radius a^* in a monovalent electrolyte under an applied electric field with magnitude E_∞^* . Here, $k_B^* T^* / e^*$ is the thermal voltage, where k_B^* is the Boltzmann constant, T^* is the absolute temperature, and e^* is the elementary charge. For reference, the thermal voltage is approximately 25 mV at $T^* = 298$ K. Variables decorated by an asterisk are dimensional quantities. Other useful parameters to characterize different regimes in electrophoresis are the dimensionless Debye layer thickness $\delta = 1 / (\kappa^* a^*)$ and the dimensionless surface charge density $\sigma = e^* a^* \sigma^* / \epsilon^* k_B^* T^*$. Here, $1 / \kappa^*$ is the Debye length, σ^* is the dimensional surface charge density, and ϵ^* is the fluid permittivity. For example, the thin-Debye-layer limit, $\delta \ll 1$, is relevant to micron-sized colloidal particles in aqueous electrolytes at millimolar (and higher) concentrations. Here, Schnitzer & Yariv (2012*b*) define $\sigma = O(1)$ as a moderately charged particle, and $\sigma = O(\delta^{-1})$ as a highly charged particle.

Initial developments on the theory of electrophoresis were made by Smoluchowski (1903), who formulated his famous equation

$$U^* = \frac{\epsilon^* \zeta^* E_\infty^*}{\eta^*}, \tag{1.1}$$

which establishes a linear relation between the steady electrophoretic velocity U^* of the particle and the imposed (steady, uniform) electric field E_∞^* , where ζ^* is the zeta potential of the colloid in a given electrolytic solution, and η^* is the dynamic viscosity of the fluid. Smoluchowski's equation is valid when the Debye length is small compared to the particle size, and for moderately charged particles, $\sigma = O(1)$. An equivalent expression for a fixed surface charge on the particle is

$$U^* = \frac{\sigma^* E_\infty^*}{\kappa^* \eta^*}, \tag{1.2}$$

in which case it is evident that the electrophoretic velocity is asymptotically small in the thin-Debye-layer limit. Furthermore, Smoluchowski's derivation of this equation assumes the weak-field limit, $\beta \ll 1$. Further developments by Debye & Hückel (1924) for thick Debye layers, $\delta \gg 1$, and Henry (1931) for arbitrary δ , also found linear relations between the particle velocity and the applied electric field, since these too assumed the weak-field limit. Specifically, the Hückel result in terms of charge density is

$$U^* = \frac{2a^* \sigma^* E_\infty^*}{3\eta^*}. \tag{1.3}$$

Overbeek (1943) and Booth (1950) included ionic convection in the electrokinetic model for electrophoresis, which accounts for relaxation effects that arise due to a relative motion between the colloid and the ions, albeit only for moderately charged particles. Numerical results by Wiersema, Loeb & Overbeek (1966) and O'Brien & White (1978), including retardation and relaxation effects for highly charged particles, followed. Here, by 'relaxation' we refer to deformation of the charge cloud from its spherically symmetric equilibrium state, and by 'retardation' we refer to a reduction in the electrophoretic speed in comparison to Smoluchowski's result. These works showed, in particular, that the electrophoretic velocity does not remain a linear function of the zeta potential for particles of sufficiently high surface charge in the weak-field limit. In the thin-Debye-layer regime, this deviation from linearity can be interpreted as being caused by surface conduction of ions in the Debye layer. Indeed, perturbation analyses by Dukhin & Semnikhin (1970) and O'Brien & Hunter (1981) allowed for a correction to Smoluchowski's formula in

binary electrolytes for thin Debye layers, owing to surface conduction; this was later generalized to multi-component electrolytes by O'Brien (1983). However, just as in the earlier developments in the theory of electrophoresis, the focus remained in the weak-field regime, $\beta \ll 1$, where the particle velocity remains linear in electric field strength.

An asymptotic analysis for nonlinear electrophoretic motion of highly charged particles in the thin-Debye-layer limit ($\delta \ll 1$) was developed by Schnitzer & Yariv (2012*b*). Here, by nonlinear electrophoresis we refer to conditions where β is not much smaller than unity, i.e. beyond the weak-field limit. Specifically, they created a macroscale model for moderate electric fields, corresponding to $\beta = O(1)$, wherein the Debye-scale transport is coarse-grained into effective boundary conditions on the equations governing the electrostatic potential and neutral salt concentration in the electroneutral bulk electrolyte outside the Debye layer. The potential and salt evolution in the bulk is also coupled to bulk fluid flow via the Stokes equations with a Coulomb body force. Using this macroscale model, they calculated the electrophoretic velocity of a spherical particle in the 'weakly nonlinear regime' as a perturbation expansion in β (Schnitzer *et al.* 2013), for $\sigma = O(\delta^{-1})$ and arbitrary Dukhin number Du . The latter quantity is a measure of the surface conductivity relative to bulk conductivity, and is defined as

$$Du = \delta^2 \sigma (1 + 2\alpha^-), \tag{1.4}$$

in which α^- is the counterion drag coefficient. The difference between our definition of Du and the one given by Schnitzer *et al.* (2013) lies in the different normalization of the surface charge density. In this weakly nonlinear regime, they found that the first nonlinear contribution to the electrophoretic velocity is of order β^3 . In a subsequent paper (Schnitzer & Yariv 2014), they analysed their macroscale model at small Du across the transition from weak to strong fields. Here, the field dependence of the nonlinear electrophoretic velocity is parametrized via the Péclet number $Pe = \alpha \zeta_0 \beta$, which physically represents the relative importance of ion advection to diffusion; α is the mean ionic drag coefficient, and ζ_0 is the dimensionless equilibrium zeta potential (normalized by the thermal voltage), defined via

$$\sigma = 2\delta^{-1} \sinh(\zeta_0/2). \tag{1.5}$$

The nonlinear electrophoretic velocity scales as β^3 at small Pe , and as $\beta^{3/2}$ at large Pe . While analytical results are not available in the transition between these two regimes, numerical computations suggest a smooth transition of the electrophoretic velocity between these limiting cases.

Experiments on nonlinear electrophoresis have confirmed that the electrophoretic velocity has a nonlinear dependence on the field strength at sufficiently large applied fields. Tottori *et al.* (2019) conducted experiments, as well as COMSOL simulations, involving highly charged submicron particles in the weakly nonlinear regime: their results are in good agreement with Schnitzer *et al.* (2013). Cardenas-Benitez *et al.* (2020) performed experiments in direct current (DC) insulator-based dielectrophoresis microfluidic devices, and attributed the observed reversal of the particle velocity direction when subjected to strong DC fields to a nonlinear electrophoretic mobility, instead of dielectrophoretic effects. Antunez-Vela *et al.* (2020) used this set-up to determine experimentally the field strength at which the electrophoretic particle velocity balances particle advection due to electro-osmotic flow in the microchannel, resulting in particle trapping. Kumar *et al.* (2006) developed a microfluidic technique to measure the electrophoretic velocity at large field strengths; in contrast to the above-mentioned studies, their results show the linear theory of electrophoresis extends beyond the weak-field regime in the case

of moderately charged particles. This is in line with Schnitzer & Yariv (2012*b*), who demonstrated that Smoluchowski's formula is indeed valid at $\beta = O(1)$ for moderately charged particles. In fact, these authors in an earlier work (Schnitzer & Yariv 2012*c*) demonstrated that Smoluchowski's formula holds until strong fields, where $\beta = O(\delta^{-1})$. This last conclusion, however, could be invalidated by consideration of dielectric–solid polarization at strong fields (Schnitzer & Yariv 2012*a*).

Theoretical and numerical results for nonlinear electrophoresis beyond the thin-Debye-layer limit are relatively scarce. Khair (2018) developed an asymptotic approximation to the nonlinear electrophoretic velocity for weakly charged colloids ($\sigma \ll 1$) with thick Debye layers ($\delta \gg 1$). It was predicted that in the strong-field regime, the electrophoretic velocity approaches Hückel's result as the Debye cloud is stripped from the particle at large β . Interestingly, the notion of Debye cloud stripping was suggested by Stotz (1978) in his experimental study of nonlinear electrophoresis in a non-polar fluid. Numerical computations from Fixman & Jagannathan (1983), using a multipole expansion to solve the full electrokinetic equations, showed no nonlinear dependence of the electrophoretic velocity on field strength at $\beta = O(1)$ for particles with $\zeta^* = O(k_B^* T^*/e^*)$. Computations from Bhattacharyya & Gopmandal (2011) for the hydrodynamic drag force on a charged particle exhibited a nonlinear dependence on field strength, at sufficiently large fields. Numerical results from Frants *et al.* (2021) in the thin-Debye-layer limit suggested a transition to an unsteady, and eventually chaotic, flow in very strong steady fields, i.e. $\beta \gg 1$, due to the formation of unstable microvortices, which lose their steadiness as the electric field increases.

In general, the nonlinear coupling between the ion concentration, the electric field and the fluid flow around the particle means that a numerical scheme must be used to compute nonlinear electrophoresis outside the weak-field regime for arbitrary Debye lengths. In the present work, a robust numerical scheme, employing a spectral element method algorithm, is developed to compute the electrophoretic velocity of a spherical, dielectric, rigid, uniformly charged particle immersed in a monovalent electrolyte for, in principle, arbitrary Debye lengths and electric field magnitudes. Additionally, the permittivity of the particle is assumed to be small compared to that of the electrolyte, which obviates the need to determine the electric potential variation within the particle. Note that this assumption is reasonable for colloidal particles of inorganic composition (e.g. silica or polystyrene) in aqueous solutions. The following sections are structured as follows. In § 2, the electrokinetic governing equations and the model assumptions are introduced. In § 3, the numerical scheme is described. In § 4, results for moderately charged and highly charged particles are presented, wherein comparisons between the present work and previous theoretical and experimental studies are made. Finally, in § 5, we offer concluding remarks and suggestions for future work.

2. Problem formulation

Consider a spherical colloidal particle freely suspended in a monovalent electrolyte solution, as shown in figure 1. Depending on the physico-chemical nature of the colloid–electrolyte interface, the particle may acquire a non-zero charge on its surface at equilibrium. To compensate this surface charge, an ion cloud richer in counterions will form around the colloid. This so-called Debye cloud, or layer, is characterized by a thickness, the Debye length $1/\kappa^* = \sqrt{\epsilon^* k_B^* T^*/2(e^*)^2 c_\infty^*}$, where c_∞^* is the bulk electrolyte concentration far from the particle. For example, $1/\kappa^*$ is approximately 10 nm for a 1 mM

Nonlinear electrophoresis of a colloidal particle

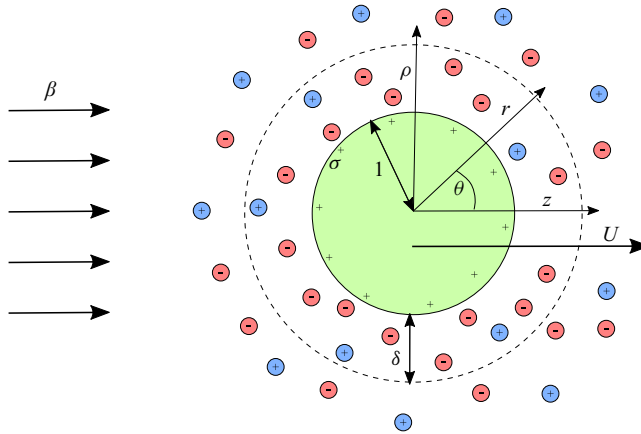


Figure 1. Diagram of a colloidal particle with positive surface charge density σ and a Debye layer of thickness δ suspended in an electrolyte, moving at electrophoretic speed U , under the influence of an applied electric field with dimensionless strength β . The main goal is to calculate U with prescribed values of δ , σ and β .

aqueous solution of a monovalent electrolyte at 298 K. Normalizing this Debye length by the particle radius a^* results in the dimensionless Debye layer thickness $\delta = 1/(\kappa^* a^*)$. For an isothermal system, δ is a function of only the particle radius and the bulk electrolyte concentration. Thin Debye layers ($\delta \ll 1$) are present in the case of large colloids or highly concentrated electrolytes. In contrast, when the colloids are small or in case of diluted solutions, this corresponds to the thick Debye layer ($\delta \gg 1$) regime. If an electric field with dimensionless strength β is imposed, then the colloid will move at a speed U along the same axis as the applied electric field. Here, $U = (e^*/k_B^* T^*)^2 \eta^* a^* U^*/\epsilon^*$ is the dimensionless electrophoretic speed, and U^* is its dimensional form. From figure 1, the surface charge is depicted as positive without loss of generality; therefore the cations and anions correspond to the coions and counterions, respectively.

To determine U , one must solve the electrokinetic equations, which encompass coupled fluid flow, ion transport and electric fields. Since we are interested in the steady-state particle velocity, we disregard the time dependence in these governing equations. Changes in temperature that would lead to variations in the physical properties of the electrolyte are neglected. Thus the system is isothermal and time-invariant. The governing equations will be presented in dimensionless form. The electric potential, ion concentration and velocity are normalized by the factors $k_B^* T^*/e^*$, c_∞^* and $\epsilon^* (k_B^* T^*/e^*)^2 / \eta^* a^*$, respectively, while the pressure and stress tensors are normalized by the Maxwell scale $\epsilon^* (k_B^* T^*/a^* e^*)^2$.

The conditions under which colloidal electrophoresis occurs correspond to an electro-quasi-static regime, meaning that all induced magnetic effects can be neglected safely. Hence the electric field in the electrolyte is governed by the Poisson equation

$$\delta^2 \nabla^2 \varphi = -\frac{1}{2}(c^+ - c^-), \quad (2.1)$$

where φ is the dimensionless electric potential and c^\pm stands for the dimensionless ion concentration, with the positive (negative) sign for cations (anions). The right-hand side of (2.1) represents the negative of the ionic charge density. The fluid flow is governed by

the continuity and Stokes equations,

$$\nabla \cdot \mathbf{u} = 0, \tag{2.2}$$

$$-\nabla p + \nabla^2 \mathbf{u} - \frac{c^+ - c^-}{2\delta^2} \nabla \varphi = \mathbf{0}, \tag{2.3}$$

where \mathbf{u} is the dimensionless fluid velocity field and p is the dimensionless pressure. Equation (2.3) excludes the inertia term; this is valid as long as the Reynolds number is small, which is a plausible assumption for micron-scale colloidal particles in aqueous solutions, moving at speeds less than approximately 1 cm s^{-1} . The last term in (2.3) is the Coulomb body force that acts on any non-electroneutral fluid element.

The ion concentration is governed by the stationary ion mass balance, i.e. the steady-state Nernst–Planck equations

$$\nabla^2 c^\pm \pm \nabla \cdot (c^\pm \nabla \varphi) - \alpha^\pm \mathbf{u} \cdot \nabla c^\pm = 0. \tag{2.4}$$

The three terms in (2.4) represent, from left to right, diffusion, electromigration and advection, respectively. The parameter $\alpha^\pm = \epsilon^* (k_B^* T^* / e^*)^2 / D^\pm \eta^*$ is the ion drag coefficient, where D^\pm is the ion diffusion coefficient. Values of α^\pm in an aqueous solution at 298 K are in the range 0.1–2 for most common systems (Vanysek 1993).

For application of the boundary conditions, it is convenient to work in a reference frame that translates with the particle speed U . In this case, the particle is stationary, and the fluid far from the particle moves at speed $-U$. We assume that the surface charge distribution on the colloid remains fixed as the imposed electric field varies in magnitude. Therefore, the inner boundary condition for the electric potential corresponds to the Gauss law at the colloid surface,

$$\mathbf{n} \cdot \nabla \varphi = -\sigma \quad \text{at } r = 1, \tag{2.5}$$

where \mathbf{n} is an outward unit vector normal to the colloid surface, and r is the radial distance in spherical coordinates with origin at the centre of the colloid. We neglect the electric field variation inside the colloid in (2.5) due to the assumed small ratio of particle to fluid permittivity.

For the fluid flow problem we assume no-slip, and for the Nernst–Planck equations we impose the no-flux condition through the colloid, namely,

$$\mathbf{u} = \mathbf{0} \quad \text{and} \quad \mathbf{n} \cdot [\nabla c^\pm \pm c^\pm \nabla \varphi] = 0 \quad \text{at } r = 1. \tag{2.6}$$

The advection term in (2.4) does not contribute to the no-flux condition in the co-moving reference frame because of the no-slip condition.

Far from the colloid, the electric field tends to the imposed electric field E_∞ , and the ion concentration must be equal to the bulk concentration c_∞ to satisfy electroneutrality at the bulk. In dimensionless form, we have

$$\nabla \varphi \rightarrow -\beta \hat{\mathbf{z}} \quad \text{and} \quad c^\pm \rightarrow 1 \quad \text{as } r \rightarrow \infty, \tag{2.7}$$

where $\hat{\mathbf{z}}$ denotes the unit vector corresponding to the axis in which the electric field is applied. Since the reference frame is moving with the colloid, the far-field boundary condition for the flow problem is

$$\mathbf{u} \rightarrow -U \hat{\mathbf{z}} \quad \text{as } r \rightarrow \infty, \tag{2.8}$$

where U is the electrophoretic speed. This value is unknown *a priori*; in fact, it is the main goal of the calculation. Since the system is at steady state, we find U by enforcing zero net

force on the particle:

$$\oint_S (\mathbf{N} + \mathbf{M}) \cdot \mathbf{n} \, dS = \mathbf{0}, \quad (2.9)$$

where \mathbf{N} and \mathbf{M} are the dimensionless hydrodynamic and Maxwell stress tensors, respectively, i.e.

$$\mathbf{N} = -p\mathbf{I} + [\nabla\mathbf{u} + (\nabla\mathbf{u})^T], \quad (2.10)$$

$$\mathbf{M} = \nabla\varphi \nabla\varphi - \frac{1}{2}(\nabla\varphi \cdot \nabla\varphi)\mathbf{I}. \quad (2.11)$$

Here, \mathbf{I} denotes the identity tensor, and the superscript T denotes the transpose. By applying the divergence theorem to (2.9), we see that $\mathbf{N} + \mathbf{M}$ must be divergence-free, therefore S in (2.9) is an arbitrary surface of integration enclosing the particle; we choose the particle surface $r = 1$ as S .

The nonlinearity in the governing equations stemming from the Coulomb force in (2.3), and the electromigration and advection terms in (2.4), as well as electromigration in the no-flux boundary condition, means that a numerical approach is generally necessary to explore the regimes of nonlinear electrophoresis.

3. Numerical formulation

Our numerical approach to find the electrophoretic speed of the particle proceeds in two steps. First, a solution of the electrokinetic equations is found, given a guess of the electrophoretic speed, by employing a spectral element method algorithm, adapted from Chisholm *et al.* (2016). Then the electrophoretic speed is computed by imposing (2.9), given a solution for φ , c^\pm and \mathbf{u} from the previous step in the system domain. The final solution is found by performing these two steps iteratively until convergence is reached within a prescribed tolerance.

The first step is solved by employing a spectral element method approach and the Galerkin method of weighted residuals (Karniadakis & Sherwin 2005). This requires the use of high-order polynomials for both the trial and test functions to achieve the desired spectral convergence. In addition, both trial and test spaces must be equal for the Galerkin method. The two-dimensional basis set is defined as a tensor product of one-dimensional Lagrange polynomials of order N , which leads to $(N + 1)^2$ degrees of freedom for each element. Finally, Gauss–Lobatto quadrature is employed to integrate over each parametric $[-1, 1]^2$ subdomain. The reader is referred to Chisholm *et al.* (2016) for more details of this numerical approach.

Due to the geometry of the system, we can benefit from the symmetry around the axis of the applied field; the azimuthal dependence of the variables involved is dropped, and the model is simplified to an axisymmetric two-dimensional problem. By exploiting this feature, (2.2) and (2.3) can be cast into the more convenient vorticity–streamfunction formulation:

$$E^2\psi + \omega = 0, \quad (3.1)$$

$$2\delta^2 \nabla^2 \omega - \nabla(c^+ - c^-) \times \nabla\varphi = \mathbf{0}, \quad (3.2)$$

in which $\omega = \nabla \times \mathbf{u}$ is the vorticity field, ω is its azimuthal (and only non-zero) component, ψ is the streamfunction, and E^2 is a second-order differential operator.

In cylindrical coordinates (z, ρ) , in which z corresponds to the symmetry axis and ρ is the normal distance to this axis, E^2 is defined as

$$E^2 = \frac{1}{\rho} \left(\frac{\partial^2}{\partial \rho^2} - \frac{1}{\rho} \frac{\partial}{\partial \rho} + \frac{\partial^2}{\partial z^2} \right). \tag{3.3}$$

The relation between the streamfunction ψ and the velocity field \mathbf{u} in cylindrical coordinates is given by

$$\mathbf{u} = \frac{1}{\rho} \left(\frac{\partial \psi}{\partial \rho} \hat{\mathbf{z}} - \frac{\partial \psi}{\partial z} \hat{\boldsymbol{\rho}} \right), \tag{3.4}$$

where $\hat{\boldsymbol{\rho}}$ is the unit vector normal to the axis of symmetry. A cylindrical coordinates system is selected to facilitate the transition to the Cartesian parametric space. The singularity at the symmetry axis introduced by this coordinate system can be circumvented with Dirichlet boundary conditions for ψ at the symmetry axis. The flow boundary conditions (2.6) and (2.8) in the vorticity–streamfunction formulation become

$$\psi = A \quad \text{at } r = 1, \tag{3.5}$$

$$\omega \rightarrow 0 \quad \text{as } r \rightarrow \infty, \tag{3.6}$$

$$\mathbf{n} \cdot \nabla \psi \rightarrow -U\rho \sin \theta \quad \text{as } r \rightarrow \infty, \tag{3.7}$$

where A is an arbitrary constant; $A = 0$ is chosen for convenience.

By taking the inner product of (2.1), (2.4), (3.1) and (3.2) with the test functions ϕ , we obtain the weak formulation of the full electrokinetic equations:

$$2\delta^2 [\langle \nabla \phi, \nabla \varphi \rangle - \langle \phi, \mathbf{n} \cdot \nabla \varphi \rangle_{\partial}] - \langle \phi, c^+ - c^- \rangle = 0, \tag{3.8}$$

$$\left\langle \nabla \phi, \nabla c^{\pm} \pm c^{\pm} \nabla \varphi - \frac{\alpha^{\pm}}{\rho} c^{\pm} \nabla^{\perp} \psi \right\rangle - \left\langle \phi, \mathbf{n} \cdot \left(\nabla c^{\pm} \pm c^{\pm} \nabla \varphi - \frac{\alpha^{\pm}}{\rho} c^{\pm} \nabla \psi \right) \right\rangle_{\partial} = 0, \tag{3.9}$$

$$\langle \nabla \phi, \nabla \psi \rangle + \left\langle \phi, \frac{2}{\rho} \frac{\partial \psi}{\partial \rho} - \rho \omega \right\rangle - \langle \phi, \mathbf{n} \cdot \nabla \psi \rangle_{\partial} = 0, \tag{3.10}$$

$$2\delta^2 \left[\langle \nabla \phi, \nabla \omega \rangle + \frac{1}{\rho^2} \langle \phi, \omega \rangle - \langle \phi, \mathbf{n} \cdot \nabla \omega \rangle_{\partial} \right] + \langle \phi, \nabla (c^+ - c^-) \times \nabla \varphi \rangle = 0. \tag{3.11}$$

Here, the angle brackets denote the inner product. Equations (3.8)–(3.11) correspond to the Poisson, Nernst–Planck, vorticity definition and vorticity transport equations, respectively, in cylindrical coordinates. The subscript ∂ denotes a boundary integral, which is evaluated only at the particle surface, the axis of symmetry and the boundary far from the particle. The second-order terms are converted to first order plus a boundary term by integrating by parts and making use of the divergence theorem.

Direct implementation of (3.8)–(3.11) would result in unnecessary computation at each step. To alleviate this issue, we define operators that can be fully defined once at the beginning of the computation, namely, $\mathbb{M}_{ij} = \langle H_i, H_j \rangle$, $\mathbb{L}_{ij} = \langle \nabla H_i, \nabla H_j \rangle$, $\mathbb{B}_{ijk} = \langle H_i, H_j \nabla H_k \rangle$, $\mathbb{D}_{ijk} = \langle H_i, \nabla H_j \times \nabla H_k \rangle$, $\mathbb{L}_{ij}^V = \mathbb{L}_{ij} + \langle H_i, H_j \rangle / \rho^2$, $\mathbb{A}_{ijk} = \langle \nabla H_i, H_j \nabla H_k \rangle / \rho$ and $\mathbb{E}_{ij}^2 = \mathbb{L}_{ij} + 2\langle H_i, \partial H_j / \partial \rho \rangle / \rho$. Here, H_i corresponds to the shape functions of the test functions ϕ , while $H_{j,k}$ are the shape functions of the variables

of interest, namely, φ , c^\pm , ω and ψ . This yields

$$2\delta^2 \mathbb{L}_{ij} \varphi_j - \mathbb{M}_{ij} (c^+ - c^-)_j = 0, \tag{3.12}$$

$$\pm \mathbb{B}_{ijk} c_j^\pm \varphi_k + \mathbb{L}_{ij} c_j^\pm - \alpha_\pm \mathbb{A}_{ijk} c_j^\pm \psi_k = 0, \tag{3.13}$$

$$\rho \mathbb{M}_{ij} \omega_j - \mathbb{E}_{ij}^2 \psi_j = 0, \tag{3.14}$$

$$2\delta^2 \mathbb{L}_{ij}^V \omega_j + \mathbb{D}_{ijk} (c^+ - c^-)_j \varphi_k = 0. \tag{3.15}$$

Equations (3.12)–(3.15) are the residuals of the discretized electrokinetic equations in index notation. The solution to this linear–bilinear system of equations is found by the Newton–Raphson algorithm. The Jacobian matrix is built by the appropriate tensor contraction, exploiting the bilinearity of the equations. The method is deemed to have converged when the L^2 -norm of the difference of successive iterations of every system variable is below a given tolerance.

The second step is finding the electrophoretic speed U , given a solution for the variables φ , c^\pm , ω and ψ . This is done iteratively using a secant method for interpolation and imposing that the total force \mathbf{F} on the particle equals zero, i.e. using (2.9). Because of axisymmetry, $F_z = \hat{z} \cdot \mathbf{F}$ is the only component of \mathbf{F} that can be non-zero with a given solution from the spectral element method algorithm. Therefore, this is the only component considered for the secant iteration. The interpolation expression is

$$U_{n+1} = \frac{F_{z,n-1} U_n - F_{z,n} U_{n-1}}{F_{z,n-1} - F_{z,n}}, \tag{3.16}$$

which requires two different speed estimates at the beginning of the computation. A tolerance of 10^{-3} was chosen in our computations to balance accuracy with instability in the secant step. The latter can occur for tolerances that are too small.

The force on the particle is calculated using (2.9). The Maxwell stress tensor \mathbf{M} can be computed readily with the solution domain for φ using (2.11). However, the hydrodynamic stress tensor in (2.10) cannot be implemented directly without an expression for the pressure. An equivalent expression for the hydrodynamic force in terms of ω , c^\pm and φ is

$$\oint \mathbf{N} \cdot \mathbf{n} \, dS = \pi \hat{z} \int_0^\pi \left[2\delta^2 \left(\frac{\partial(r\omega)}{\partial r} - 2\omega \right) - (c^+ - c^-) \frac{\partial\varphi}{\partial\theta} \right] \sin^2 \theta \, d\theta. \tag{3.17}$$

Equation (3.17) is the drag calculation for a spherical particle in a steady axisymmetric flow, adapted from Khair & Chisholm (2014), with an additional term that takes into account the effect of the Coulomb body force on the hydrodynamic pressure. Here, r and θ are spherical coordinates, such that $z = r \cos \theta$ and $\rho = r \sin \theta$.

The computational mesh is generated using Gmsh (Geuzaine & Remacle 2009), with a spherical half-ring configuration of inner radius $R_i = 1$ and outer radius $R_o = 100$. Lagrange polynomials of order $N = 8$ were employed as basis sets, and 9×9 quadrilateral elements were selected. The elements were distributed throughout 20^2 nodes in both the r and θ directions. In the radial direction, a geometric progression outwards with factor 1.25 was employed, while in the θ direction, factor 1.1 was used from 0 to $\pi/2$, and from π to $\pi/2$. This created a mesh with a greater number of elements near the surface of the colloid and the symmetry axis, as shown in figure 2, with the smallest element size being 0.289. The tolerance for the Newton–Raphson step was set to 10^{-5} , while the tolerance for the secant method was set to 10^{-3} . An irrotational flow with a uniform electric field and

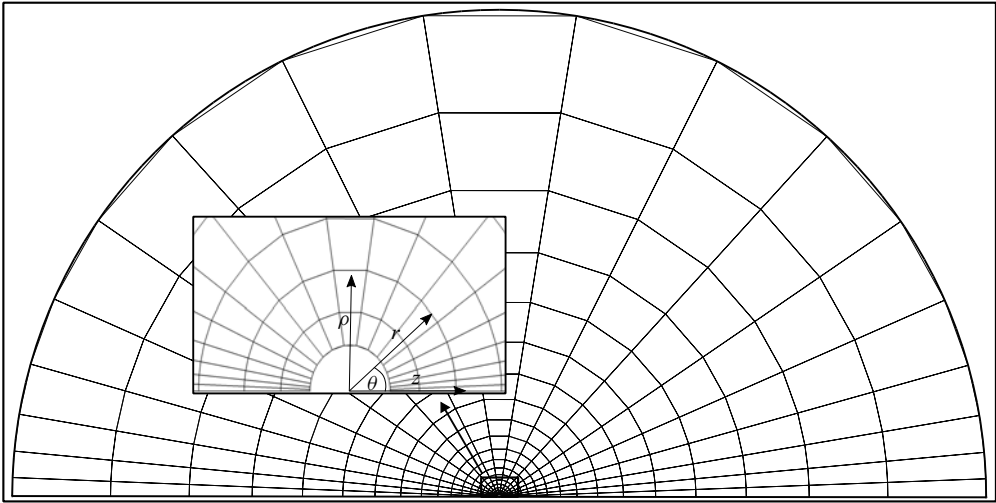


Figure 2. Computational mesh with half-ring configuration, in which the number of nodes is set to 20^2 , with outward radial progression 1.25, and angular progression 1.1 towards $\theta = \pi/2$. The inset shows a closer view of the mesh near the particle surface $r = 1$.

zero charge density was used as the initial condition. Finally, the initial speed guesses were $U_0 = 0$ and $U_1 = \sigma\beta$ for each simulation. Convergence computations for different values of β and δ to justify the chosen R_o and the number of nodes are provided in [Appendix A](#).

4. Results and discussion

4.1. Moderately charged particles, $\sigma = O(1)$

To examine the nonlinear electrophoretic speed dependence of a moderately charged particle on the electric field strength, numerical calculations are conducted for $\sigma = 1$ and $\alpha^\pm = 0.3$. We sweep through the parameters δ and β in the domains $[0.05, 10]$ for δ and $[10^{-1}, 10^3]$ for β . This means that our computations cover thick and thin Debye layers, as well as weak and strong fields. For the smallest values of δ , the number of elements was increased, such that the smallest element size was 0.031. In principle, the mesh could be refined, to allow computations for smaller values of δ , which would translate into longer computation times.

[Figure 3](#) illustrates the scaled electrophoretic mobility, defined as

$$\mu = \frac{3U}{2\sigma\beta}, \tag{4.1}$$

as a function of the field strength β for different Debye layer thicknesses δ . The electrophoretic mobility can be viewed as the ratio of speed to field strength, and it is scaled in such a way that the Hückel limit corresponds to a horizontal line at $\mu = 1$. Recall that Hückel derived this result for a particle with a thick Debye layer ($\delta \gg 1$) in a weak field ($\beta \ll 1$). Physically, in this limit, electrokinetic effects associated with the deformation of the Debye cloud are absent; the electrophoretic speed is found simply by balancing the electric force on the particle, equal to its total charge multiplied by the electric field, with the Stokes drag on the sphere. The electrophoretic speed is linear with the electric field when the curves in [figure 3](#) are horizontal; or equivalently, the mobility is independent of field strength. The weak-field regime ($\beta \ll 1$) is thus characterized by a mobility that is

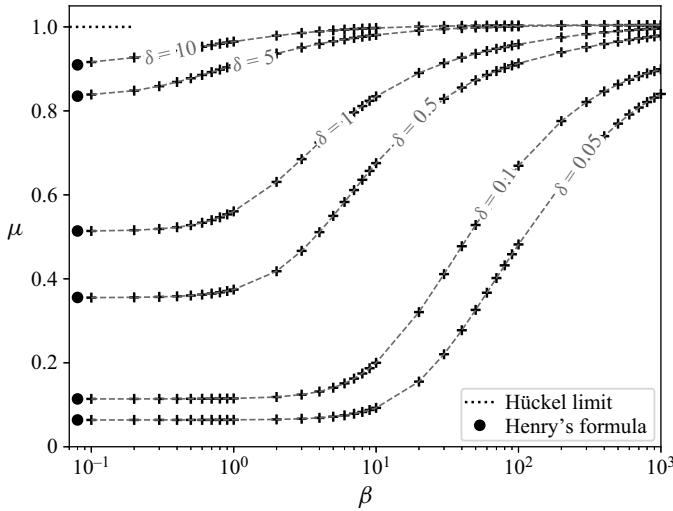


Figure 3. Scaled electrophoretic mobility μ (see (4.1)) of a moderately charged particle versus β for different values of δ . Here, $\sigma = 1$ and $\alpha^\pm = 0.3$. Symbols correspond to the numerical computations, while the connecting lines are for visual purposes only.

independent of β but dependent on δ , since the speed is linear in the field strength. Here, our computations are in good agreement with Henry (1931).

At larger values of β , the electrophoretic mobility transitions to a nonlinear regime, deviating from Henry's result with a superlinear behaviour. Figure 3 shows that the value of β at which this nonlinear regime starts is δ -dependent: for instance, the linear behaviour is maintained up to $\beta \approx O(\delta^{-1})$ for $\delta \ll 1$, which is consistent with the asymptotic results from Schnitzer & Yariv (2012c) and also the experimental observations of Kumar *et al.* (2006). This confirms that Smoluchowski's formula in the thin-Debye-layer limit holds beyond the weak-field regime.

At large values of β , an inflection point appears and the nonlinear contribution to the mobility shifts to a sublinear trend. Eventually, as β increases, another linear regime is reached. Remarkably, regardless of the value of δ , the electrophoretic mobility appears to approach the Hückel limit as $\beta \rightarrow \infty$. This regime is reached even at relatively moderate values of β in the case $\delta > 1$. It is worthwhile revisiting the assumption that the Reynolds number Re is negligibly small at large field strengths. Here, $Re = 2\rho^*\epsilon^*(k_B^*T^*/e^*)^2\sigma\beta\mu/3(\eta^*)^2$, where ρ^* is the fluid density. This expression is obtained using the electrophoretic speed as the velocity scale and the respective normalizing factors introduced in § 2. However, the highest value of Re in our computations is $Re = 0.3$, in the case $\sigma = \mu = 1$ and $\beta = 10^3$. This value is not negligible, but it is sufficiently small for the Stokes equations to provide a plausible approximation to the flow around the particle. In summary, as the electric field strength increases, the electrophoretic speed transitions from a linear variation with β characterized by Henry's formula to a nonlinear (superlinear) variation that is δ -dependent, and finally to another linear variation at the Hückel limit.

Figure 4 shows a comparison of our numerical results with the asymptotic prediction for the mobility from Khair (2018), valid for thick Debye layers ($\delta \gg 1$) and symmetric electrolytes ($\alpha^+ = \alpha^- = \alpha$). In the present notation, that expression reads

$$\mu = 1 - \frac{3}{2} \frac{L(Pe)}{\delta} + O(\delta^{-2}), \tag{4.2}$$

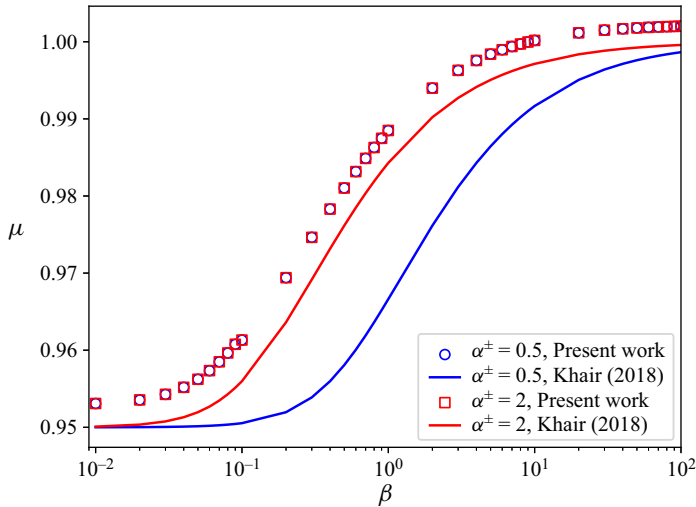


Figure 4. Comparison of the scaled electrophoretic mobility μ (see (4.1)) as a function of β for $\delta = 20$ and $\sigma = 1$. Symbols correspond to our numerical computations, while lines correspond to the asymptotic expression from Khair (2018). Note that the squares and circles essentially lie on top of one another, which indicates that the numerical results are insensitive to the value of α^\pm , in contrast to the asymptotics of Khair (2018).

$$L(Pe) = \frac{1}{Pe} \left[\left(2 + \frac{4}{Pe^2} \right) \coth^{-1} \left(\sqrt{1 + \frac{4}{Pe^2}} \right) - \sqrt{1 + \frac{4}{Pe^2}} \right], \quad (4.3)$$

in which $Pe = 2\alpha\delta\sigma\beta/3$ is a Péclet number, proportional to the dimensionless field strength. As $\beta \rightarrow \infty$, both the numerical and asymptotic results approach the Hückel limit for large values of δ . However, our numerical computations differ from Khair (2018) in the sensitivity to α^\pm . In the case of the numerical solution, the mobility for both cases of α^\pm is essentially the same for any value of β . This results in a better agreement when $\alpha^\pm = 2$; meanwhile, when $\alpha^\pm = 0.5$, the numerics and the asymptotics differ significantly. One might suspect that this discrepancy could be attributed to the Coulomb body force term in the Stokes equation, which is accounted for in our numerics but neglected in Khair (2018). The neglect of that term is valid provided that $Pe \gg \delta^{-2}$, as discussed in Khair (2018) – see (19) in that paper. Note that $Pe \gg \delta^{-2}$ even for the smallest values of β and α^\pm in figure 4, which is sufficient to neglect the electrical body force. The error in (4.2) is of order δ^{-2} , and this seems to be consistent with the mismatch between numerics and theory in figure 4.

Figure 5 displays the charge $\frac{1}{2}(c^+ - c^-)$, ionic strength $\frac{1}{2}(c^+ + c^-)$ and counterion c^- density configurations around the particle for $\delta = 1$ at weak, moderate and strong, field regimes. Figures 5(a–c) show that the charge distribution is essentially spherically symmetric around the particle when $\beta = 0.1$, characteristic of a weak perturbation to the equilibrium Debye cloud around a uniformly charged particle. The charge in this cloud is negative since $\sigma > 0$. At $\beta = 5$, the charge distribution has lost its spherical symmetry and displays a slight fore–aft asymmetry, and the Debye cloud appears to be closer to the particle surface when compared to the weak-field regime. At $\beta = 50$, the spherical asymmetry is increased, and the electric field has stripped the Debye layer from the colloid. The fact that the Debye layer is stripped from the particle in strong

Nonlinear electrophoresis of a colloidal particle

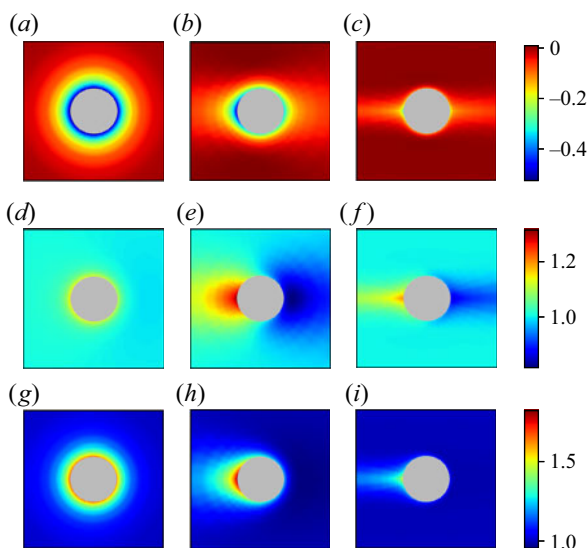


Figure 5. (a–c) Charge, (d–f) ionic strength, and (g–i) counterion density distributions around the particle in (a,d,g) weak, $\beta = 0.1$, (b,e,h) moderate, $\beta = 5$, and (c,f,i) strong, $\beta = 50$, electric fields for $\delta = \sigma = 1$ and $\alpha^{\pm} = 0.3$.

electric fields explains why the electrophoretic mobility approaches the Hückel limit, since the electrokinetic retardation provoked by the Debye cloud becomes less prominent. Notably, the contribution from the electric dipole to the overall electric field, which at large distances is dominated by the imposed field, continues to be small, even after losing spherical symmetry, due to the maintained fore–aft symmetry.

Figures 5(d–f) illustrate the ionic strength for the same values of δ and β , where it can be seen that the spherical symmetry is broken when β is not small. However, there is a different behaviour between the left and right sides of the particle. Since the particle is moving, to the right in figure 5, there are relaxation effects that become more significant at large values of β , making the ion cloud lag behind the particle as it moves. Figures 5(g–i) show the counterion distribution around the colloid. When comparing to the ionic strength, we see that the lack of ions to the right of the particle is not due to counterions. Notably, this asymmetric – in both spherical and fore–aft characteristics – counterion density distribution was proposed by O’Brien & White (1978), due to a disparity in the motion (relative to the particle) of the counterions at the front and at the rear of the colloid. This disparity causes the counterions to spend more time behind the particle as the latter moves. Since the colloid is only moderately charged, the coions also play an important role to reduce the fore–aft asymmetry in the charge density distribution.

Figure 6 shows the velocity field for varying values of the ion drag coefficient α^{\pm} and electric field strength β . Here, $\alpha^{+} = \alpha^{-}$, as probably best approximated by KCl. Note, however, that our numerical scheme can readily handle cases where the ionic diffusion coefficients are unequal, although this is not explored in the present work. Increasing the ion drag coefficient α^{\pm} has a slight effect on the flow, skewing the streamlines opposite to the particle direction of motion. This would result in a retardation effect, slowing down the particle. It can also be seen that this effect is more noticeable in stronger fields, where the nonlinearity is more prevalent.

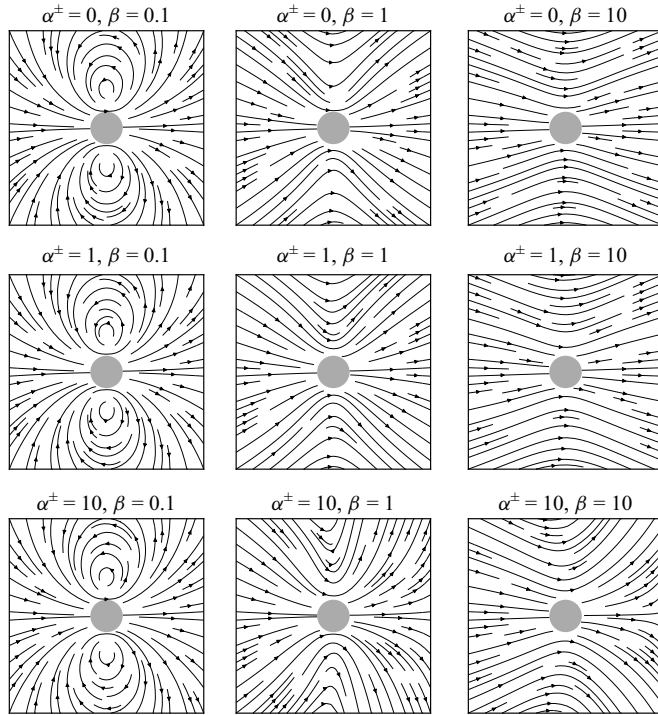


Figure 6. Streamlines of the velocity for different values of the ion drag coefficient α^\pm and electric field strength β . Here, $\delta = \sigma = 1$.

The impact of β on the flow is more noticeable; [figure 6](#) illustrates the transition between a flow pattern, at the particle scale, characteristic of phoretic motion to a flow pattern due to a conservative force. Namely, when $\beta = 0.1$, a velocity field with a (irrotational) source dipole characteristic is visible, suggesting that the flow disturbance by the particle decays as $1/r^3$. This is the classic flow pattern for electrophoretic motion of a particle under a weak field, agreeing with the potential flow solution derived originally by Morrison (1970) and Anderson (1989) under the assumption of a thin Debye layer ($\delta \ll 1$) and a moderately charged particle ($\sigma = O(1)$). Schnitzer & Yariv (2012c) removed the weak-field restriction and showed that this potential flow solution holds for fields up to $\beta = O(\delta^{-1})$. Notably, our computations suggest that the potential flow structure persists at the particle scale ($r = O(1)$) even beyond the small- δ limit. In the weak-field regime, α^\pm has a negligible effect on the flow patterns. However, as β increases, the effect of α^\pm is evident. When $\beta = 1$, the source dipole is lost to some degree. Finally, when $\beta = 10$, the flow pattern resembles a sedimentation flow profile, where the flow disturbance is longer-ranged, decaying as $1/r$. This is related tightly to the ion cloud distribution shown in [figure 5](#); as the electric field gets stronger, the Debye layer gets stripped from the colloid, reducing the magnitude of the coupling between the flow, ion transport and electric field, which leads to a conservative body force in the flow momentum equation. The important implication is that the common notion of hydrodynamic interactions between moderately charged particles undergoing electrophoresis being weak is invalidated at sufficiently strong fields. That is, at strong fields, the $1/r$ velocity decay at the particle scale would result in hydrodynamic interactions similar to particles undergoing sedimentation, for example.

The present discussion has focused on the flow profile and ion distributions at the particle scale. In [Appendix A](#), we present results for how the disturbance to the applied electric field varies at large distances from the particle. The results therein confirm that a sedimentation flow profile is attained at large β .

4.2. Highly charged particles, $\sigma \gg 1$

For the case of highly charged particles, a refinement in the computational mesh was imperative to obtain converging results. The high charge on the colloid exacerbates the presence of the boundary layer at the Debye scale, leading to numerical errors with the above-mentioned number of nodes. Convergence was reached when using 40^2 nodes distributed using the same radial and angular progressions after an adaptive mesh refinement. This resulted in a mesh with size 0.004 in the particle neighbourhood. Furthermore, due to the small size of the Debye layer, visual depictions of the ion cloud, as in [figure 5](#), are difficult to make; hence we focus on computing the electrophoretic velocity and comparing it to known results.

[Figure 7](#) shows a comparison to the asymptotic expression from Schnitzer & Yariv (2014) obtained from analysis of their thin-Debye-layer macroscale model at small Du (see (1.4)) and small α^\pm . They refer to the latter condition as a ‘small-ion’ approximation, which means that the Péclet number is also small. The comparison is performed on the deviation from Smoluchowski’s formula; that is, we compute the field-dependent mobility

$$\mu_1 = \frac{1}{Du} \left(\frac{U}{\beta} - \zeta_0 \right). \quad (4.4)$$

Here, ζ_0 is the zeta potential at weak electric fields and negligible ionic polarization, and it is related to the surface charge density by $\zeta_0 = 2 \ln(\delta\sigma)$. The small-ion asymptotic expression from Schnitzer & Yariv (2014) is given by

$$\mu_1 = -4 \ln \left(\cosh \frac{\zeta_0}{4} \right) - \zeta_0 + \frac{2}{21} \beta^2. \quad (4.5)$$

The first two terms in (4.5) address the inadequacy of Smoluchowski’s formula in the case of highly charged particles in weak fields, while the last term represents the nonlinearity of the electrophoretic mobility in field strength. Our numerical computations and (4.5) exhibit the transition of the ion cloud from acting as a retardation effect to an enhancement, to the overall electrophoretic velocity as β increases. This is evidenced by the sign change of μ_1 with increasing β in [figure 7](#). We view this agreement as a validation of our numerical computations. We stop our computations at $\beta = 10$ to avoid numerical instabilities that arise at stronger fields. These instabilities can be managed by using a finer mesh, which would lead to larger computation times.

This transition from retardation to enhancement is not restricted to thin Debye layers: it also appears in the case $\delta = O(1)$, as shown in [figure 8\(a\)](#). For low values of σ , the mobility transitions from Henry’s formula to a superlinear behaviour as was shown in [figure 3](#); and the electrophoretic mobilities for $\sigma = 0.1$ and $\sigma = 1$ remain close for any value of β . However, for a more highly charged particle ($\sigma = 10$ in the figure), the mobility in the weak-field regime is lower than the value predicted by Henry, then it transitions smoothly to an enhanced mobility as β increases; this is in line with the prediction of Schnitzer & Yariv (2014) for thin Debye layers.

[Figure 8\(b\)](#) also displays how increasing σ causes a reduction in the mobility at weak-to-moderate electric field strength. However, in the strong field regime, increasing

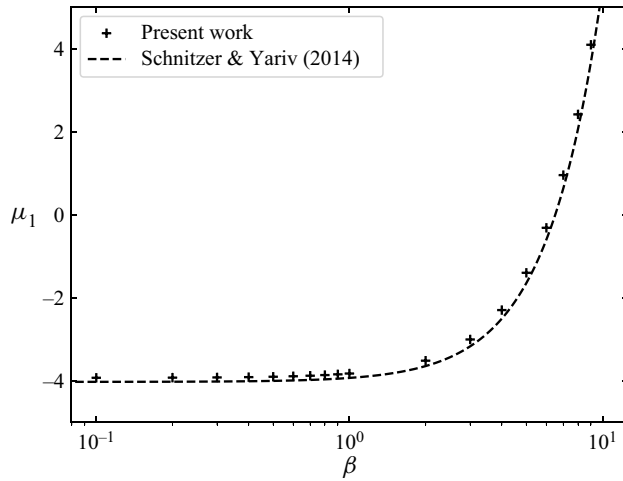


Figure 7. Comparison of the electrophoretic mobility deviation μ_1 (see (4.4)) from Smoluchowski's formula to the small-ion asymptotic expression from Schnitzer & Yariv (2014) in (4.5). Here, $\delta = 0.02$, $\sigma = 213$, $\alpha^\pm = 0.01$, $\zeta_0 = 3$ and $Du = 0.1$.

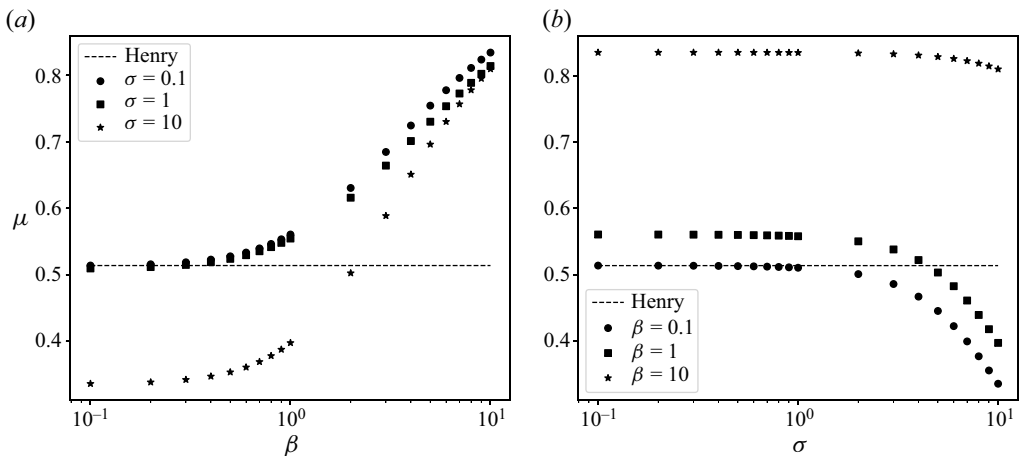


Figure 8. Scaled electrophoretic mobility μ (see (4.1)) versus (a) β at different values of σ , and (b) σ at different values of β . Here, $\delta = 1$ and $\alpha^\pm = 0.3$.

the surface charge σ has only a slight effect on the mobility, since this is already approaching Hückel's result.

The comparisons in figures 7 and 8 were made with specific values of δ . In the comparison to Schnitzer & Yariv (2014) in figure 7 for $\delta = 0.02$, a retardation effect of the Debye cloud (i.e. negative μ_1) is still seen at $\beta = O(1)$. Thus in this case, a weak-field response is seen even at non-small values of β . This is not true for the case of $\delta = 1$ as shown in figures 3 and 8. Therefore, the transition from retardation to enhancement is also δ -dependent, as was the case of the departure from the linear electrophoretic velocity.

Figure 9 illustrates the effect of α^\pm on the nonlinear contribution to the electrophoretic velocity. The comparison is made in the nonlinear contribution to the electrophoretic speed U_{nl} ; this is obtained by subtracting the linear speed U_l from the total velocity U . The linear speed is calculated as $U_l = \mu_0\beta$, where μ_0 is approximated as the total electrophoretic

Nonlinear electrophoresis of a colloidal particle

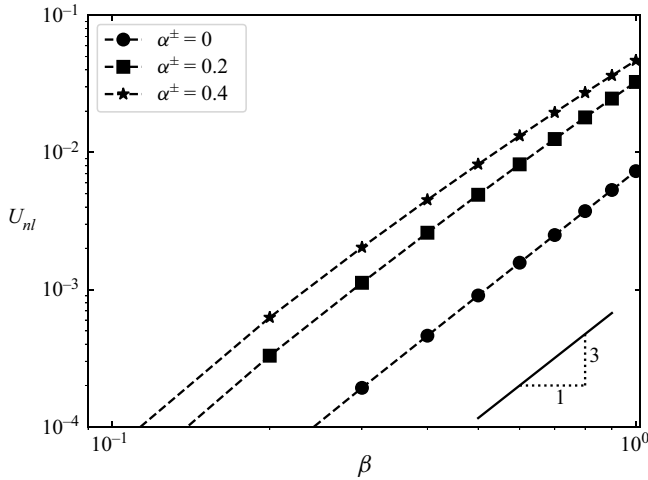


Figure 9. Nonlinear electrophoretic velocity U_{nl} for different values of α^\pm . Here, $\delta = 0.02$, $\sigma = 213$ and $\zeta_0 = 3$. The connecting dashed lines are for visual purposes only.

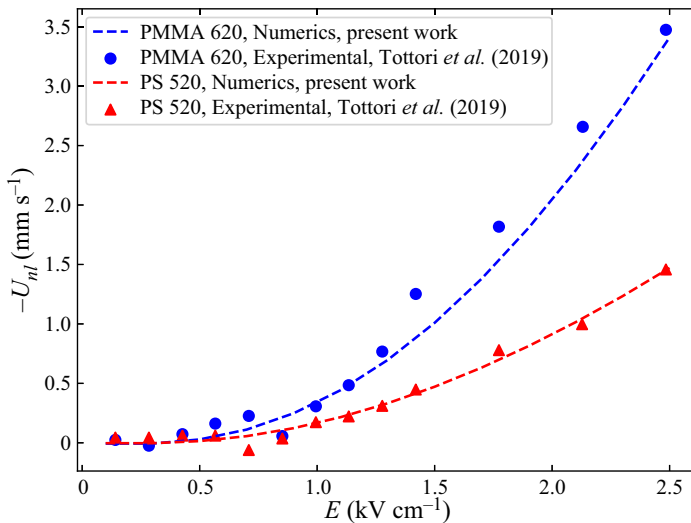


Figure 10. Comparison of the nonlinear electrophoretic velocity U_{nl} with experimental results from Tottori *et al.* (2019). Blue: PMMA particles with $\delta = 0.03$, $\beta_{max} = 3$, $\sigma = -890$, $\alpha^\pm = 0.45$, $\zeta_0 = -6.5$. Red: PS particles with $\delta = 0.04$, $\beta_{max} = 2.5$, $\sigma = -190$, $\alpha^\pm = 0.45$, $\zeta_0 = -4$.

mobility at $\beta = 10^{-2}$. The slope of all three curves is approximately 3 over the range of β examined, with a small deviation for larger values of β and α^\pm . This is in good agreement with the weakly nonlinear analysis (Schnitzer *et al.* 2013), since the leading behaviour of U_{nl} is $O(\beta^3)$. Furthermore, at fixed β , U_{nl} increases with increasing α^\pm (over the range of α^\pm examined), in agreement with Schnitzer & Yariv (2014).

A comparison to experimental results from Tottori *et al.* (2019) is presented in figure 10. Those authors measured the speed of polystyrene (PS) and polymethyl methacrylate (PMMA) particles immersed in a KCl solution in a microfluidic channel. The particles move due to a combination of electrophoresis and advection in an electro-osmotic flow

resulting from the charged channel walls. The comparison is made in the nonlinear contribution to the electrophoretic speed; here, the linear component of the speed encompasses both linear electro-osmotic and electrophoretic components. Our numerical predictions are in good agreement with the experiments for both PMMA and PS particles. In both cases, the thin Debye layer represents a mathematical boundary layer, wherein the ionic concentrations and electric potential vary rapidly, making numerical computations challenging. Just as for the comparisons in [figure 7](#), a refinement in the mesh was necessary to obtain converging results, especially in the case of PMMA particles. Their experiments for both particles correspond to the thin-Debye-layer limit, both particles are highly charged, and the field strength is weak to moderate. More specifically, in the case of PMMA particles, $\delta = 0.03$, $\beta_{max} = 3$, $\sigma = -890$, $\alpha^{\pm} = 0.45$ and $\zeta_0 = -6.5$; while for PS particles, $\delta = 0.04$, $\beta_{max} = 2.5$, $\sigma = -190$, $\alpha^{\pm} = 0.45$ and $\zeta_0 = -4$. The values of δ and β_{max} are approximately the same for both particles; however, PMMA particles have a significantly larger σ than PS particles, resulting in more prominent nonlinear electrophoresis (and more challenging computations).

5. Conclusion

We have presented a numerical technique to compute the electrophoretic velocity of a uniformly charged, spherical, rigid, dielectric particle for, in principle, arbitrary Debye length and electric field strength. Specifically, we developed a spectral element method to solve the full nonlinear electrokinetics to this end. For moderately charged particles, we showed that the electrophoretic mobility transitions smoothly from Henry's formula to a superlinear mobility with increasing β . Regardless of the value of δ , the electrophoretic mobility tends to the Hückel limit for sufficiently large values of β . However, the rate of this transition to the Hückel limit in strong fields is δ -dependent. In addition, we demonstrated how the fluid flow around the particle transitions from a phoretic-like pattern in weak fields to that induced by a conservative force when $\beta \gg 1$. In the case of highly charged particles, our results compare well with previous experiments and asymptotic expressions. We corroborated the transition of the Debye cloud from retardation to enhancement of particle motion, as predicted by Schnitzer & Yariv (2014), and we showed that this behaviour is not exclusive to thin Debye layers.

Future work naturally follows, as the numerical technique can be modified to capture the transient behaviour of the electrophoretic velocity, which is of paramount importance when the particle is under the influence of alternating fields, for example. The present numerical scheme can also be expanded to take into account electrothermal effects in the electrokinetic equations, which could become prominent at large values of β , by incorporating an energy equation, to determine the evolution of the temperature distribution around the particle. Finally, other electrostatic conditions at the particle surface would be of interest, beyond the fixed-charge assumption adopted here. For example, a natural extension would be to consider particles with surface charge regulation.

Funding. This work was supported by the National Science Foundation through grant no. CBET 2002120.

Declaration of interests. The authors report no conflict of interest.

Author ORCIDs.

 Richard Cobos <https://orcid.org/0000-0002-6035-6370>;

 Aditya S. Khair <https://orcid.org/0000-0001-6076-2910>.

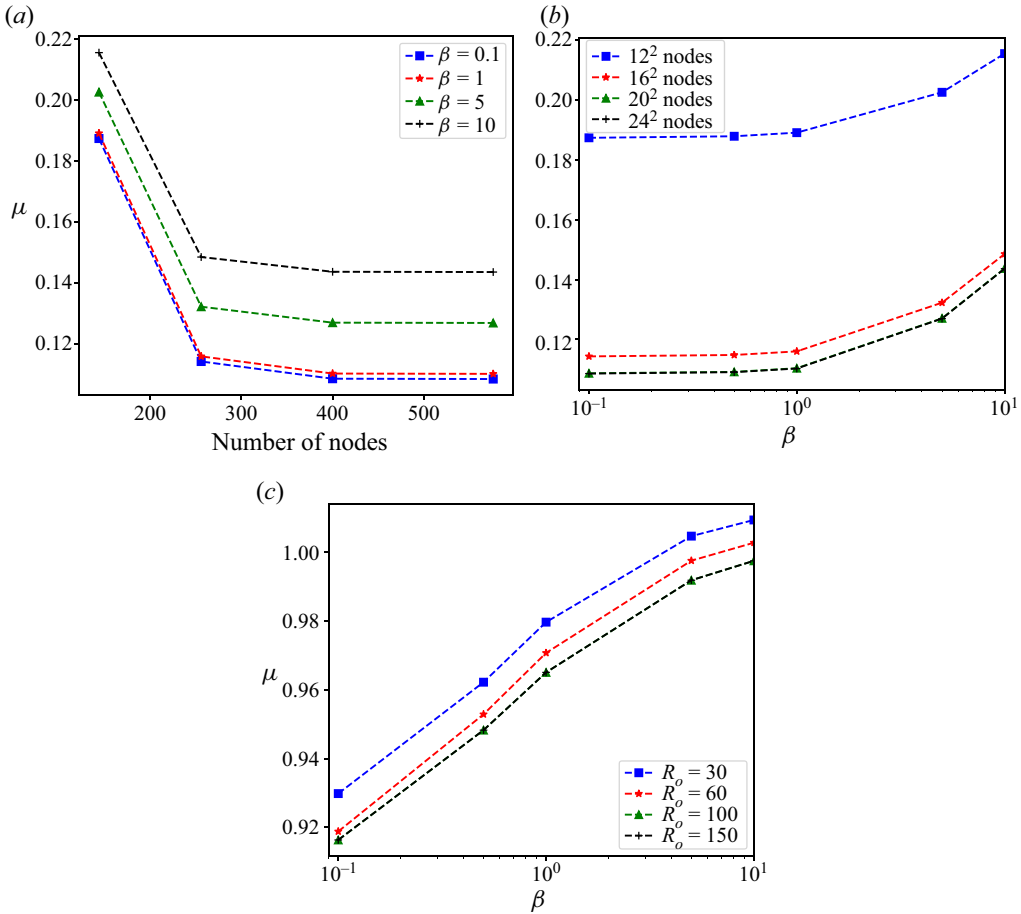


Figure 11. Convergence test of the electrophoretic mobility at weak-to-moderate fields with different numbers of nodes and values of R_o . Here, $\sigma = 1$ and $\alpha^\pm = 0.4$.

Appendix A. Convergence test and electric field far from the particle

Figure 11 shows a convergence test to determine the number of nodes and the size of the domain. A thin Debye layer ($\delta = 0.1$) was used as a test case to determine the number of nodes, and a thick Debye layer ($\delta = 10$) was used to determine the size of the domain R_o . These test cases were chosen as they represent the worst-case scenarios for each of these two parameters. Figure 11(a) illustrates the exponential convergence with increasing number of nodes for different values of β . While varying the number of elements (figure 11b), the domain size was fixed at $R_o = 100$, and when varying the domain size (figure 11c), the number of nodes was 20^2 . Figure 11 illustrates that the improvement, of choosing a finer mesh or a larger domain than the chosen values, is negligible in the case of moderately charged particles.

Figure 12 displays contours of the negative of the charge density for $\delta = \sigma = 1$ and $\alpha^\pm = 0.3$, for $\beta = 0.1, 1, 10$ and 50 . The same value of charge density $c^+ - c^- = 10^{-2}$ is chosen in each case. At weak fields ($\beta = 0.1$ in the figure), the charge density is essentially isotropic. However, as β increases, the contour extends in the field direction. Hence for large β , it is critical to choose the domain size R_o to be sufficiently large to capture the field-driven extension of the charge cloud. For these computations, $R_o = 100$.

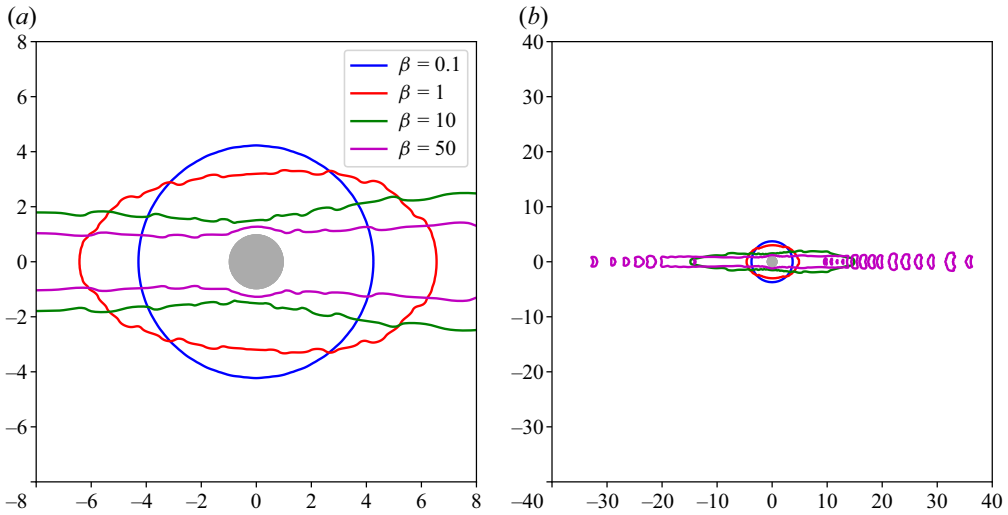


Figure 12. Contour plot of charge density distribution for $\delta = \sigma = 1$ and $\alpha^\pm = 0.3$, (a) close to the particle, and (b) far from the particle. Contours levels correspond to $c^+ - c^- = 10^{-2}$. Since the particle is positively charged, this corresponds to the negative of the charge density in the electrolyte.

With reference to figure 11(c), this value of R_o results in a calculation of the mobility that does not change appreciably if R_o is increased further.

It is also of interest to determine how the disturbance to the uniform applied field varies at large distances from the particle. Following Fixman & Jagannathan (1983), the electric potential can be written as the multipole expansion

$$\varphi = -\beta z + \frac{1}{8\pi\delta^2 r} \left[q + \frac{1}{r^2} \mathbf{p} \cdot \mathbf{r} + O(r^{-2}) \right], \tag{A1}$$

where q is the apparent charge (or monopole strength), and \mathbf{p} is the charge dipole. Note that $\mathbf{p} = p\hat{z}$ due to axisymmetry, where p is the dipole strength. We can calculate these quantities from our numerical scheme as the volume integrals

$$q = 8\pi\delta^2\sigma + \int (c^+ - c^-) dV \quad \text{and} \quad \mathbf{p} = \int (c^+ - c^-) \mathbf{r} dV, \tag{A2a,b}$$

where the first term in the monopole strength is the contribution from the charge on the particle surface.

Figures 13(a) and 13(b) show the monopole and dipole strengths, respectively, for $\delta = \sigma = 1$ and $\alpha^\pm = 0.4$ over the range $\beta = 10^{-2}$ to $\beta = 10^2$. Interestingly, the monopole contribution is generally non-zero, although it is small for weak fields. This is in agreement with numerics from Fixman & Jagannathan (1983). We compute a change in sign of the monopole strength with increasing β , which was also reported in their paper (see their figure 1), although their computations were restricted to values of β smaller than ours. The existence of a monopole contribution to the disturbance field implies that a net electric force F_e is exerted on a spherical surface at large distances from the particle. In figure 13(c), we compute this electric force (i.e. the surface integral of the traction arising from the Maxwell stress) over the surface $R_o = 100$. The electric force is small at weak fields but certainly not negligible at moderate and large β . Schnitzer & Yariv (2014) noted that a net electric force can exist on a surface enclosing the Debye layer and particle for thin

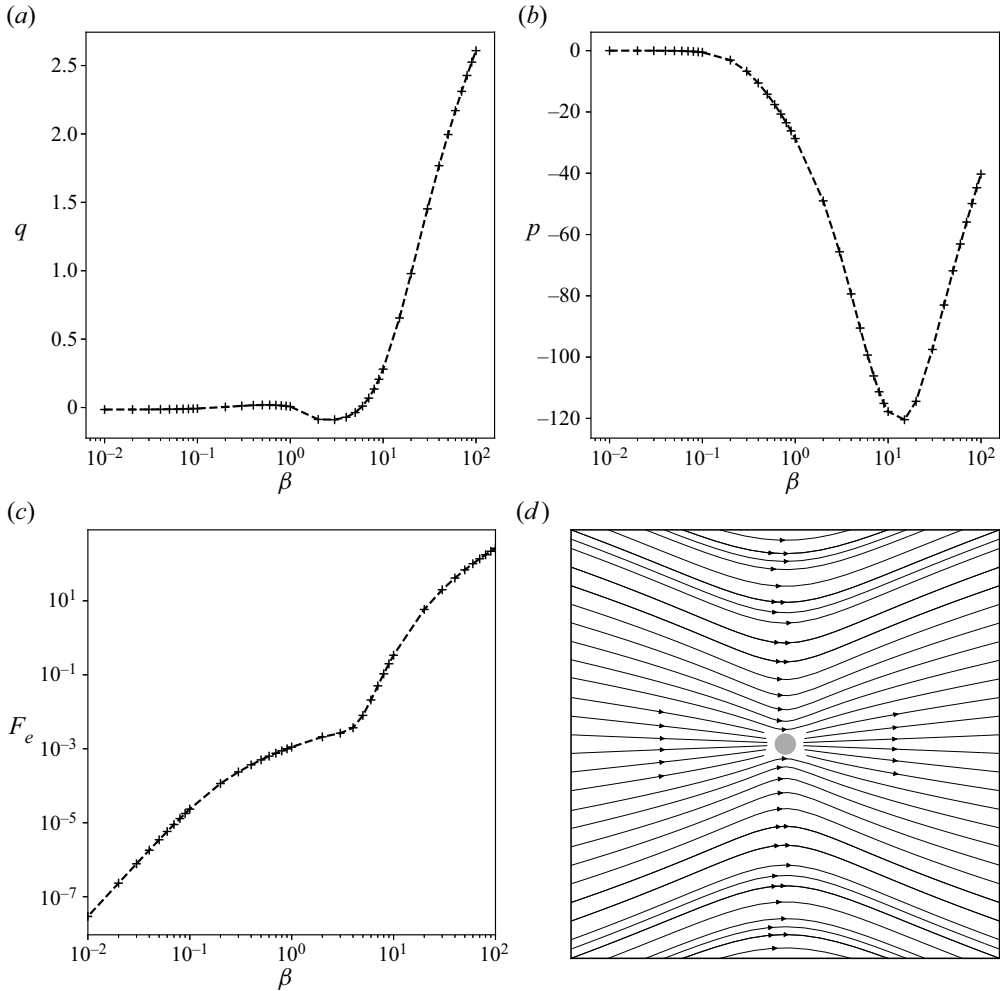


Figure 13. (a) Monopole strength q , (b) dipole strength p , and (c) electric force F_e , evaluated using a far-field radius $r = 100$. (d) Velocity streamlines for the case $\beta = 50$. Here, $\delta = \sigma = 1$ and $\alpha^\pm = 0.4$.

Debye layers beyond the weak field limit. Since the system must be force-free (see (2.9)), a non-zero electric force over R_o must be compensated by a non-zero hydrodynamic force. Thus at large distances we expect the velocity field to decay as a Stokeslet; figure 13(d) shows the streamlines around the particle, which displays the familiar pattern associated with a particle under a net hydrodynamic force. The dipole strength (which is negative) decreases initially with increasing β , again in a manner that is similar to that found in Fixman & Jagannathan (1983). We find a minimum in the dipole strength at $\beta \approx 10$, which is beyond the field strength that they examined.

REFERENCES

- ANDERSON, J.L. 1989 Colloid transport by interfacial forces. *Annu. Rev. Fluid Mech.* **21** (1), 61–99.
 ANTUNEZ-VELA, S., PEREZ-GONZALEZ, V.H., DE PEÑA, A.C., LENTZ, C.J. & LAPIZCO-ENCINAS, B.H. 2020 Simultaneous determination of linear and nonlinear electrophoretic mobilities of cells and microparticles. *Anal. Chem.* **92** (22), 14885–14891.

- BHATTACHARYYA, S. & GOPMANDAL, P.P. 2011 Migration of a charged sphere at an arbitrary velocity in an axial electric field. *Colloids Surf. (A)* **390** (1–3), 86–94.
- BOOTH, F. 1950 The cataphoresis of spherical, solid non-conducting particles in a symmetrical electrolyte. *Proc. R. Soc. Lond. A* **203** (1075), 514–533.
- CARDENAS-BENITEZ, B., JIND, B., GALLO-VILLANUEVA, R.C., MARTINEZ-CHAPA, S.O., LAPIZCO-ENCINAS, B.H. & PEREZ-GONZALEZ, V.H. 2020 Direct current electrokinetic particle trapping in insulator-based microfluidics: theory and experiments. *Anal. Chem.* **92** (19), 12871–12879.
- CHISHOLM, N.G., LEGENDRE, D., LAUGA, E. & KHAIR, A.S. 2016 A squirmer across Reynolds numbers. *J. Fluid Mech.* **796**, 233–256.
- DE CORATO, M., ARQUÉ, X., PATINO, T., ARROYO, M., SÁNCHEZ, S. & PAGONABARRAGA, I. 2020 Self-propulsion of active colloids via ion release: theory and experiments. *Phys. Rev. Lett.* **124** (10), 108001.
- DEBYE, P.J.W. & HÜCKEL, E. 1924 *Bemerkungen zu einem Satze über die kataphoretische Wanderungsgeschwindigkeit suspendierter Teilchen*. Hirzel.
- DUKHIN, S.S. & SEMENIKHIN, V.N. 1970 Theory of double layer polarization and its influence on the electrokinetic and electro-optical phenomena and the dielectric permeability of disperse systems. *Colloid J. USSR* **32** (3), 298–305.
- ERICKSON, D. & LI, D. 2004 Integrated microfluidic devices. *Anal. Chim. Acta* **507** (1), 11–26.
- FIXMAN, M. & JAGANNATHAN, S. 1983 Spherical macroions in strong fields. *Macromolecules* **16** (4), 685–699.
- FRANTS, E.A., ARTYUKHOV, D.A., KIREEVA, T.S., GANCHENKO, G.S. & DEMEKHIN, E.A. 2021 Vortex formation and separation from the surface of a charged dielectric microparticle in a strong electric field. *Fluid Dyn.* **56** (1), 134–141.
- GEUZAINÉ, C. & REMACLE, J.F. 2009 Gmsh: a 3-D finite element mesh generator with built-in pre- and post-processing facilities. *Intl J. Numer. Meth. Engng* **79** (11), 1309–1331.
- HENRY, D.C. 1931 The cataphoresis of suspended particles. Part I – the equation of cataphoresis. *Proc. R. Soc. Lond. A* **133** (821), 106–129.
- HUANG, X.C., QUESADA, M.A. & MATHIES, R.A. 1992 DNA sequencing using capillary array electrophoresis. *Anal. Chem.* **64** (18), 2149–2154.
- KARNIADAKIS, G. & SHERWIN, S. 2005 *Spectral/HP Element Methods for Computational Fluid Dynamics*. Oxford University Press.
- KHAIR, A.S. 2018 Strong deformation of the thick electric double layer around a charged particle during sedimentation or electrophoresis. *Langmuir* **34** (3), 876–885.
- KHAIR, A.S. & CHISHOLM, N.G. 2014 Expansions at small Reynolds numbers for the locomotion of a spherical squirmer. *Phys. Fluids* **26** (1), 011902.
- KUMAR, A., ELELE, E., YEKSEL, M., KHUSID, B., QIU, Z. & ACRIVOS, A. 2006 Measurements of the fluid and particle mobilities in strong electric fields. *Phys. Fluids* **18** (12), 123301.
- LIU, P. & MATHIES, R.A. 2009 Integrated microfluidic systems for high-performance genetic analysis. *Trends Biotechnol.* **27** (10), 572–581.
- MITTAL, M., LELE, P.P., KALER, E.W. & FURST, E.M. 2008 Polarization and interactions of colloidal particles in AC electric fields. *J. Chem. Phys.* **129** (6), 064513.
- MORRISON, F.A. 1970 Electrophoresis of a particle of arbitrary shape. *J. Colloid Interface Sci.* **34** (2), 210–214.
- O'BRIEN, R.W. 1983 The solution of the electrokinetic equations for colloidal particles with thin double layers. *J. Colloid Interface Sci.* **92** (1), 204–216.
- O'BRIEN, R.W. & HUNTER, R.J. 1981 The electrophoretic mobility of large colloidal particles. *Can. J. Chem.* **59** (13), 1878–1887.
- O'BRIEN, R.W. & WHITE, L.R. 1978 Electrophoretic mobility of a spherical colloidal particle. *J. Chem. Soc. Faraday Trans.* **74**, 1607–1626.
- OVERBEEK, J.T.G. 1943 Theory of the relaxation effect in electrophoresis. *Kolloide Beihefte* **54**, 287–364.
- RUSSEL, W.B., SAVILLE, D.A. & SCHOWALTER, W.R. 1991 *Colloidal Dispersions*. Cambridge University Press.
- SCHNITZER, O. & YARIV, E. 2012a Dielectric–solid polarization at strong fields: breakdown of Smoluchowski's electrophoresis formula. *Phys. Fluids* **24** (8), 082005.
- SCHNITZER, O. & YARIV, E. 2012b Macroscale description of electrokinetic flows at large zeta potentials: nonlinear surface conduction. *Phys. Rev. E* **86** (2), 021503.
- SCHNITZER, O. & YARIV, E. 2012c Strong-field electrophoresis. *J. Fluid Mech.* **701**, 333–351.
- SCHNITZER, O. & YARIV, E. 2014 Nonlinear electrophoresis at arbitrary field strengths: small-Dukhin-number analysis. *Phys. Fluids* **26** (12), 122002.

Nonlinear electrophoresis of a colloidal particle

- SCHNITZER, O., ZEYDE, R., YAVNEH, I. & YARIV, E. 2013 Weakly nonlinear electrophoresis of a highly charged colloidal particle. *Phys. Fluids* **25** (5), 052004.
- SMOLUCHOWSKI, M. 1903 Contribution à la théorie de l'endosmose électrique et de quelques phénomènes corrélatifs. *Bull. Akad. Sci. Cracovie*. **8**, 182–200.
- STOTZ, S. 1978 Field dependence of the electrophoretic mobility of particles suspended in low-conductivity liquids. *J. Colloid Interface Sci.* **65** (1), 118–130.
- TOTTORI, S., MISIUNAS, K., KEYSER, U.F. & BONTHUIS, D.J. 2019 Nonlinear electrophoresis of highly charged nonpolarizable particles. *Phys. Rev. Lett.* **123** (1), 014502.
- VANYSEK, P. 1993 *Ionic Conductivity and Diffusion at Infinite Dilution*. CRC Handbook of Chemistry and Physics, pp. 5–92. CRC Press.
- WIERSEMA, P.H., LOEB, A.L. & OVERBEEK, J.T.G. 1966 Calculation of the electrophoretic mobility of a spherical colloid particle. *J. Colloid Interface Sci.* **22** (1), 78–99.
- ZHU, Z., LU, J.J. & LIU, S. 2012 Protein separation by capillary gel electrophoresis: a review. *Anal. Chim. Acta* **709**, 21–31.